JACS
JOURNAL OF THE AMERICAN CHEMICAL SOCIETY

ARTICLE

pubs.acs.org/JACS

Role of Hydration Force in the Self-Assembly of Collagens and Amyloid Steric Zipper Filaments

Krishnakumar M. Ravikumar[†] and Wonmuk Hwang*[,†,‡]

[†]Department of Biomedical Engineering and [‡]Materials Science and Engineering Program, Texas A&M University, College Station, Texas 77843, United States

Supporting Information

ABSTRACT: In protein self-assembly, types of surfaces determine the force between them. Yet the extent to which the surrounding water contributes to this force remains as a fundamental question. Here we study three self-assembling filament systems that respectively have hydrated (collagen), dry nonpolar, and dry polar (amyloid) interfaces. Using molecular dynamics simulations, we calculate and compare local hydration maps and hydration forces. We find that the primary hydration shells are formed all over the surface, regardless of the types of the underlying amino acids. The weakly oscillating hydration force arises from coalescence and depletion of hydration shells as two filaments approach, whereas local water diffusion, orientation, or hydrogen-bonding events have no direct effect. Hydration forces between hydrated, polar, and nonpolar interfaces differ in the amplitude and phase of the oscillation relative to the equilibrium surface separation. Therefore, water-mediated interactions between these protein surfaces, ranging in character from "hydrophobic" to "hydrophilic", have a common molecular origin based on the robustly formed hydration shells, which is likely applicable to a broad range of biomolecular assemblies whose interfacial geometry is similar in length scale to those of the present study.

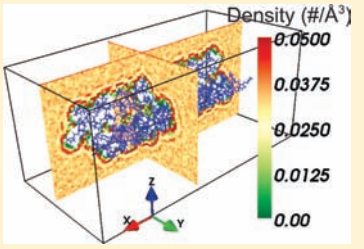

INTRODUCTION

Water-mediated forces play crucial roles in biomolecular interactions and assemblies, yet understanding their physical basis still remains a challenge.[1−5] Conventionally, they can be divided into hydrophobic and hydrophilic types, where previous theoretical modeling and computer simulations provided much insight.[1,2,5] Hydrophobic attraction between smooth or confined surfaces at close separations is known to arise from a dewetting transition driven by the solvent fluctuation at the interface,[6−8] while other effects such as polarization of water and solute or nanobubble formation may be responsible for longer-range attraction.[9−12] Between polar or charged surfaces that can form hydrogen bonds with water, the interaction can be attractive, repulsive, or oscillatory.[2,13] Such *hydration force* is believed to be due to the ordering of water into solvation (hydration) shells around the solute surface,[13,14] where resistance to the removal of water from the surface is responsible for the repulsive force.[15,16] The oscillatory behavior of the hydration force observed between macroscopically flat surfaces is due to the layering of hydration shells, which can smooth out to a monotonic profile when the surfaces are flexible.[2,14] Another possible contributor to the hydration force is the influence of the surface on the orientational distribution of water.[17]

At nanometer length scales, simulations provide atomistic pictures for water-mediated forces. However, most previous simulations used simplified surfaces such as plates, cylinders, spheres, or simplified protein structures.[15,18−20] Others employed atomistic structures focused on hydrophobic attraction.[21−24] It is unclear to what extent results for macroscopic or simpler systems can be extrapolated to biomolecular surfaces that are geometrically complex and contain various polar and nonpolar groups side-by-side. For example, a surface can change from hydrophilic to hydrophobic as its roughness increases.[25,26] A study of a model hydrophobic ligand−receptor complex even suggested that hydrophobic association, which is considered to be entropically driven, can be enthalpic in nature.[27]

Here we elucidate hydration forces in three biomolecular filament systems that self-assemble with different types of interfaces (Figure 1): collagens remain hydrated after assembly,[28−30] and the two β-sheet bilayer filaments that we study form dry interfaces that respectively have nonpolar and polar residues.[31,32] The dry interface within the bilayer is also called a "steric zipper" due to the geometric complementarity of the amino acid side chains (Figure 2b,c).[32,33] We find that, despite the presence of various amino acid side chains, hydration shells form in all cases, suggesting that the general tendency of a liquid to form high-density solvation shells near flat, rigid surfaces ("hard-wall effect")[34,35] applies for these filamentous protein surfaces. As a result, a weakly oscillating hydration force arises, regardless of the type of surface considered, where quantitative details such as the magnitude and location of the hydration repulsion or attraction, and the amplitude and phase of the hydration force, depend on the surface polarity and geometry. The present results provide a unifying picture for water-mediated interactions, where the primary hydration shell plays a central role. Thus, at the length scale of the surfaces studied here, the hydrophobic or hydrophilic nature of an interaction may not simply be a matter of the types of

Received: May 12, 2011
Published: June 22, 2011

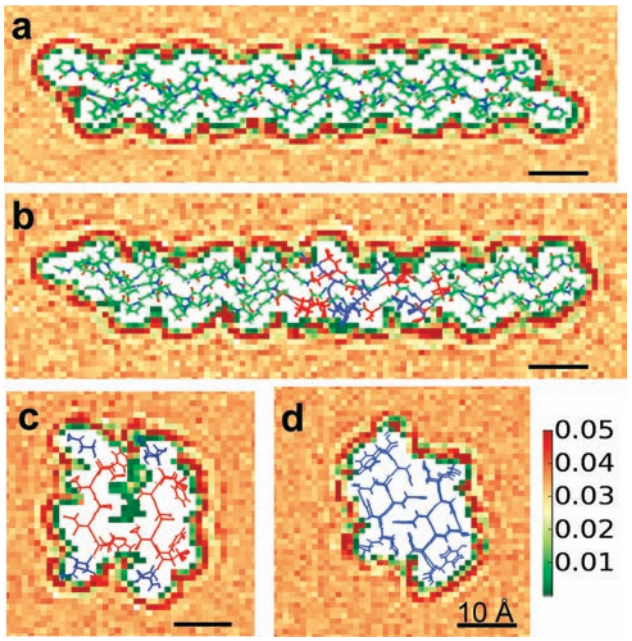

Figure 1. Water density maps (in number per Å^3): (a,b) collagen in side view and (c,d) amyloid β-sheet bilayers in axis view. Amino acids are colored blue (polar/charged), red (nonpolar), and green (collagen Gly-Pro-(hydroxy)Pro triplets). The primary hydration shell and, more faintly, the secondary hydration shell form throughout the surface, irrespective of the types of the underlying amino acids. Protein Data Bank (PDB) IDs: (a) 2D3F,[36] (b) 1BKV,[29,37] (c) 2KIB,[31] and (d) 1YJP.[32]

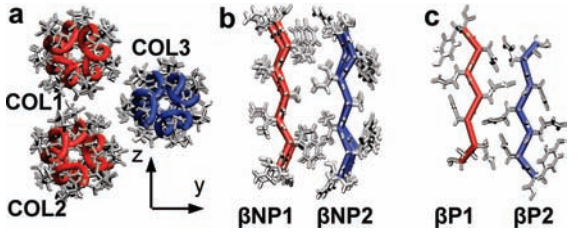

Figure 2. Cross-sectional view of the filaments used for force measurement. (a) Three 2D3F peptides. Individual collagen triple helices are named COL1−3. (b) 2KIB and (c) 1YJP. "NP" and "P" in β-sheet names stand for nonpolar and polar, respectively. Filament axes are perpendicular to the page. COL3, βNP2, and βP2 are translated in the y-direction, and forces on them during simulations are measured (see Methods). The antiparallel β-sheet 2KIB forms a "hetero zipper",[31] which is less tight compared to the interdigitation of the parallel β-sheet 1YJP.[32]

surface groups; other factors such as surface geometry, complementarity, and flexibility may also play a role for the net interaction.

METHODS

Peptides Used. We used X-ray structures of three collagen peptides, referred to by their Protein Data Bank (PDB) IDs: 2D3F,[36] 1BKV,[29,37] and 1A3I.[38] 2D3F has the sequence $(PPG)_4$-POG-$(PPG)_4$ (~8 nm long; G = glycine, P = proline, and O = hydroxyproline). The GPP and GPO triplets are the most stable structural motifs in native collagen.[29,39] We used a three-peptide 2D3F system for force measurements (Figure 2a) and a single 2D3F to show that its diffusion and conformational motion have negligible effects on the hydration maps. 1BKV has a nine-residue region containing both nonpolar and polar (including charged) residues in the middle. We used it to test hydration maps around the bulky polar and nonpolar side chains in the collagen triple helix. 1A3I has three GPP units (~2 nm long), which is less than a third the size of 2D3F or 1BKV. We used it to analyze the effect of different water models on hydration maps.

For the β-sheet bilayers, we used PDB structures 2KIB[31] and 1YJP[32] (Figure 1c,d). Unlike other X-ray structures used in our study, 2KIB is a solid-state NMR structure, and we used the first structure among the 10 in its PDB file. The amino acid sequence of 2KIB is NFGAILS, where F, A, I, and L are nonpolar. On the other hand, all residues of 1YJP (GNNQQNY) are polar. Each β-sheet forming a bilayer filament of 2KIB (1YJP) has four (five) peptides, about 1.66 nm (2 nm) in length.

Simulation Protocol. For simulation, we used the GROMACS simulation package[40] with the all-atom CHARMM Param22 force field.[41] The peptides were solvated in an orthorhombic simulation box with dimensions ranging from 45 × 45 × 45 Å^3 to 110 × 55 × 50 Å^3, depending on the size of the peptide used. We used the SPC water model for simulations of collagens and the TIP3P model for those of the β-sheet filaments. We also used the SPC/E water model to compare the calculated forces. Periodic boundary conditions were imposed. Additional force-field parameters for hydroxyproline were taken from an earlier study.[42] The system was energy minimized for 500 steps using the steepest descent method, heated from 0 K to the target temperatures (273, 300, or 330 K) for 50 ps, and equilibrated at the respective temperature for 30 ps, with all heavy atoms harmonically constrained to their original positions (spring constant $k = 10^4$ kJ/(mol·nm^2)). The final production run was performed using the leapfrog integrator with a 2-fs time step. The length of the hydrogen−heavy atom bond was fixed using the LINCS algorithm.[43] Coordinates were saved every $\Delta t = 1$ ps. The nonbonded pair and image atom lists were updated every 20 fs. A 13-Å cutoff was used for nonbonded interaction energies, and the particle mesh Ewald summation method[44] was used to calculate electrostatic interactions. Temperature and pressure were maintained using the velocity rescaling thermostat[45] and Berendesen pressure coupling.[46] Trajectories were stable during production runs, with relative root-mean-square fluctuations of temperature and energy less than 1.2%.

In simulations of 1BKV, which has a charge of +3e ($e = 1.6 \times 10^{-19}$C), we added three Cl^- ions to neutralize the net charge. The production run for each of the three-peptide 2D3F and single-peptide 1A3I simulations lasted 8 ns, while it was 4 ns for single-peptide 1BKV or 2D3F simulations. All the β-sheet simulations lasted for 8 ns. The total simulation time for the entire study was ~1.4 μs.

Hydration Map. Within each 1-Å^3 unit cell of the simulation box, we calculated the following:

Density. If a water oxygen visits the cell n times, the density is $\rho = n/n_{tot}$, where n_{tot} is the total number of saved coordinate frames.

Translational Diffusion Coefficient. For frames where a water oxygen visits the cell, we calculated its mean-square displacement during Δt (= 1 ps), $\langle \Delta l^2 \rangle = \Sigma \Delta l^2/n$. The diffusion coefficient is $D_t = \langle \Delta l^2 \rangle / 6\Delta t$. This definition gives known values of diffusion coefficients in the bulk water for the water models we tested (Figure S1).

Rotational Diffusion Coefficient. We assign three unit vectors to a water molecule: $\mathbf{r}_1$, along the water dipole; $\mathbf{r}_2$, orthogonal to $\mathbf{r}_1$ in the plane containing water atoms; and $\mathbf{r}_3 = \mathbf{r}_1 \times \mathbf{r}_2$ (Figure S2). Since $\mathbf{r}_i$ (i = 1, 2, 3) swivels on a two-dimensional unit sphere, if we denote its angular displacement during Δt by $\Delta\phi_i$, the corresponding rotational diffusion coefficient is[47] $D_{\mathbf{r}_i} = \langle \Delta\phi_i^2 \rangle / 4\Delta t$, with $\langle \Delta\phi_i^2 \rangle = \Sigma \Delta\phi_i^2/n$.

Orientation Angle. For the collagen system, the water orientation angle relative to the protein surface is the angle θ_i between $\mathbf{r}_i$ (i = 1, 2, 3) and the minimum distance vector from the collagen helical axis nearest

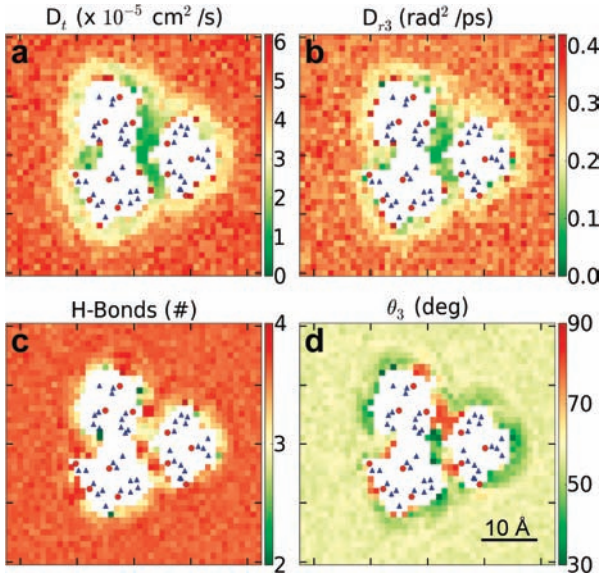

Figure 3. Cross section of hydration maps for the three-peptide 2D3F system. Hydration maps for β-sheet filaments are in Figures S4 and S5. Dots inside the protein (white region) are peptide oxygen (red circle) and carbon (blue triangle) atoms within ±1.5 Å from the cross-sectional plane. (a) Translational (D_t) and (b) rotational (D_{r3}) diffusion coefficients. (c) Average number of hydrogen bonds. (d) Average radial orientation angle (θ_3) of water, which is overall larger near surface carbonyl oxygens. The bulk value of θ_3 approaches the analytical limit; 1 rad = 57.3°. Figure S3 shows maps for other quantities.

to the water oxygen (Figure S2). The helical axis of a peptide (triple helix) passes through its center of mass and is parallel to the x-axis in Figure 2. For the β-sheet bilayers, θ_i was measured between $\mathbf{r}_i$ (i = 1, 2, 3) and the direction perpendicular to the β-sheet (y-axis in Figure 2).

Because of the symmetry of the water molecule, θ_2 and θ_3 are in the range [0°,90°]. A lower θ_2 and higher θ_3 correspond approximately to a radial orientation, as seen around the polar groups (Figures 3d, S3d, S4g, h, and S5g,h). For a randomly rotating water molecule, the average value for θ_1 ($0° \le \theta_1 \le 180°$) is 90°. On the other hand, the average for θ_2 or θ_3 is $\langle\theta_{2,3}\rangle = {}^1/_2[\int_0^{\pi/2} \theta \sin\theta \, d\theta + \int_{\pi/2}^{\pi} (\pi - \theta) \sin\theta \, d\theta] = 1$ rad. These correspond to the bulk values in the hydration maps.

Number of Hydrogen Bonds. For frames where a water molecule visits the cell, the average number of hydrogen bonds that a water molecule makes with neighboring water molecules and peptide atoms was counted with a hydrogen−oxygen distance cutoff of 2.4 Å and without any angular cutoff.[48]

The hydration map in the case without any constraint on the peptide was obtained by assigning a local coordinate frame to the cross section of the peptide[49] and defining unit cells with respect to the local frame ("No Constraint" in Figure S6).

Hydration Force. To measure intermolecular forces, the heavy atoms on one side of the filament assemblies (Figure 2, COL1, COL2, βNP1, and βP1) were restrained with spring constants $k = 10^4$ kJ/(mol·nm^2). The other part (COL3, βNP2, βP2) was translated along the y-axis by Δy_0 in 1-Å intervals. Δy_0 ranges [−4.0,+4.0] Å for the collagen and [−2.0,+10.0] Å for the β-sheets. Since collagens have a hydrated interface at the crystallographic separation ($\Delta y_0 = 0$ Å), a closer approach ($\Delta y_0 = -4.0$ Å) than the amyloid steric zipper interfaces ($\Delta y_0 = -2.0$ Å) was possible. At each Δy_0, C_α atoms of the translated part of the system were weakly constrained (k = 500 kJ/(mol·nm^2)). Denoting the number of these atoms by n_C and their average position during each 8-ns simulation by Δy, the net force per unit length of the molecule is $F_{tot} = n_C k(\Delta y - \Delta y_0)$/(peptide length) (dashed lines in Figure 4a−c). Hydration force, F_{hyd} (solid line), was obtained by subtracting from F_{tot} the average nonbonded interaction force, F_{int}, on the translated part (COL3, βNP2, and βP2) by the stationary part (Lennard-Jones and electrostatic; dotted lines in Figure 4a−c). To test the possible effect of the constraining potential on the measured force, for 2D3F, we varied its spring constant. The measured forces followed the same force profile, which suggests that the magnitude of constraints does not affect measuring the force that the molecule experiences (Figure S7).

When calculating the average separation Δy for an 8-ns simulation, we excluded the initial period during which the translated part (Figure 2) reaches its equilibrium position. For 93% of the simulations, this time was <50 ps, except for some cases of 2KIB and 1YJP, where it took 0.2−4 ns to reach the equilibrium position. Force profiles obtained from the first half and the last half of the measured intervals were nearly identical, indicating sufficient sampling time. Likewise, hydration maps were calculated on the basis of the trajectory after the initial transient.

Local Correlation Function in Thermal Motion. Using 2D3F, we tested the correlation between protein motion and the motion of nearby water molecules. We followed displacements of a water oxygen and the nearest collagen heavy atom during 1 ps and assigned unit vectors in the corresponding directions, denoted as **u** and **a**, respectively. With r representing the distance between the two atoms, we define the correlation function

$$g(r) = \langle \mathbf{u} \cdot \mathbf{a} \rangle_r \qquad (1)$$

where the average is over all water oxygen−nearest protein heavy atom pairs within the range (r,$r + \Delta r$) (Δr = 0.5 Å). For comparison, we randomly selected 20 water molecules in the bulk, measured $g(r)$ for each with the surrounding water molecules, and averaged them to obtain the water−water correlation function (Figure S8).

Effect of Water Models on Hydration Maps. We compared the hydration maps of the smaller peptide 1A3I using three different water models, SPC, TIP3P, and SPC/E. The density maps are nearly identical (Figure S1). The translational diffusion coefficient (D_t) of the SPC/E water in bulk is the closest to the experimental value (~3.1 × 10^{-5} cm^2/s), while it is higher for SPC (≈ 4.8 × 10^{-5} cm^2/s) and TIP3P (~5.8 × 10^{-5} cm^2/s), as reported earlier.[50] Similar differences in magnitude were also seen for rotational diffusion coefficients, but their profiles near the protein surface are qualitatively similar (Figure S1).

RESULTS AND DISCUSSION

General Features of the Hydration Shell. To distinguish water-mediated interactions from those caused by the conformational motion, we harmonically constrained the peptides and calculated the local water density, diffusion coefficients (translational and rotational), orientation angles relative to the protein surface, and number of hydrogen bonds at 1-Å resolution (see Methods). The resulting hydration maps (Figures 1 and 3) are nearly identical with or without the harmonic constraint (Figure S6). This is likely because hydration water organizes faster than the conformational motion of the filaments. Furthermore, directions of thermal motion of water oxygen and nearby protein heavy atoms are only weakly correlated (Figure S8). Constraining or fixing protein atoms has been previously used for elucidating the behavior of the hydration water.[21,25] The results below are thus obtained with restraints on proteins, which also allows more extensive sampling and intermolecular force measurement.

In all the systems tested, the primary hydration shell is formed regardless of the type of the underlying amino acid (Figure 1). Instead of forming a depletion zone,[2] a high-density hydration shell is also formed around the nonpolar 2KIB, as has been

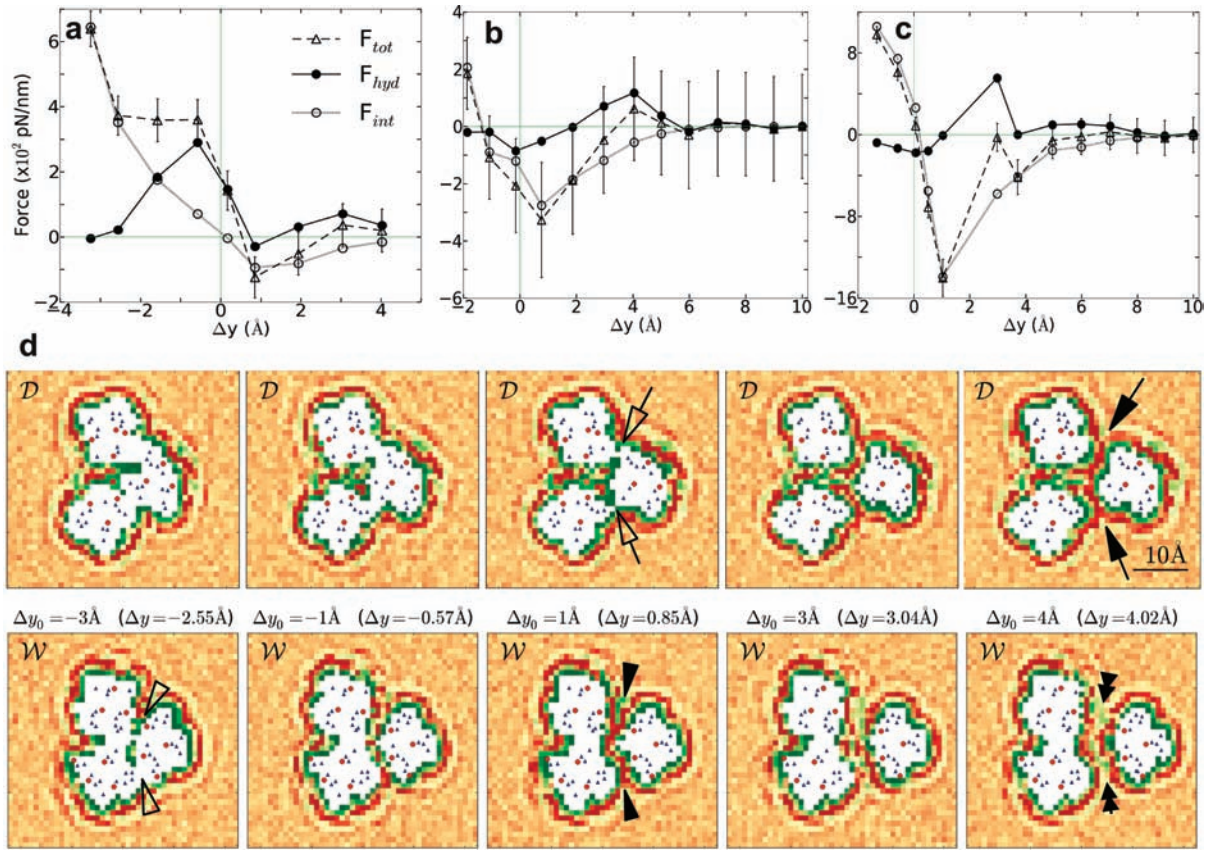

Figure 4. Relationship between hydration force and hydration map. (a−c) Forces per nanometer length of filament for (a) 2D3F, (b) 2KIB, and (c) 1YJP. F_{tot} = net force, F_{int} = interaction force directly between peptides, and F_{hyd} = hydration force. Error bars (standard deviation) are shown for F_{tot}, which are comparable in magnitude to those for F_{int} and F_{hyd}. Although F_{hyd} oscillates, the corresponding potential of mean force profile does not (Figure S11). Note that Δy at which F_{tot} = 0 pN/nm deviates the most from 0 Å in (b) for 2KIB, which is a solid-state NMR structure (see text). (d) Water density maps shown in two cross sections at different separation distances of 2D3F. The color scale is the same as in Figure 1. At the crystallographic separation (Δy_0 = 0 Å), "*D*" and "*W*" respectively denote regions with dry and wet interfaces between peptides (Figure S10). Arrows and arrowheads indicate coalescence and depletion of primary hydration shells. Peaks of the oscillating hydration force in (a) are located between these transitions (Δy_0 = −1 and 3 Å). Similar maps for β-sheet filaments are shown in Figure S12.

observed for a model spherical hydrophobe,[27] also known as the "hard-wall" effect.[34,35] The translational and rotational diffusion coefficients are 2−5-fold lower across the protein surface than in the bulk water and increase monotonically away from the surface (Figures 3a,b, S3a,b, S4a−d, and S5a−d), which is consistent with previous computational[22,51−53] and experimental studies.[54,55] These results suggest that the formation of primary hydration shells and retardation of water motion are mainly due to the boundary-induced packing effects rather than specific interactions between water molecules and particular surface groups. In the case of 2KIB, which has an antiparallel β-sheet structure, there is a low density of water within the bilayer (Figure 1c), indicating that the two β-sheets do not form the steric zipper as tightly as in 1YJP, which has parallel β-sheets (Figure 2).[56] When we performed simulation without any constraint on the filaments, the two β-sheets of 2KIB packed more closely, eliminating the interfacial water. The translational diffusion coefficient for the intersheet water molecules is low (Figure S4a), while their rotational diffusion coefficients are nearly as high as in the bulk (Figure S4b−d). Though we have fewer statistics in the low-density regions, the high rotational diffusion is likely a result of the absence of hydrogen bonds within the nonpolar interface (Figure S4e).

Unlike density and diffusion maps, the average number of hydrogen bonds between water and the protein surface is nonuniform, being higher around polar groups and lower around nonpolar groups (Figures 3c, S4e, and S5e). Retardation of water motion near the protein surface, even with a smaller average number of hydrogen bonds, suggests a glassy rather than ice-like state.[5] As a result of hydrogen bond formation, water orients with one of its OH bonds aligned radially outward from the surface around polar groups, while the orientation is circumferential near nonpolar groups, which can be seen near the surface oxygen atoms (red circles) in Figures 3c and S3c,d.[51,57,58] For the β-sheet filaments, the trend is similar, but less clear (Figures S4f−h and S5f−h). This is likely because the surface normal direction, defined relative to the plane of the β-sheet (see Methods), has poorer correlation with water orientation due to the bulkier side chains, whereas the collagen triple helix of 2D3F has a smoother surface geometry with less bulky prolines and hydroxyprolines.

Hydration Force Profile. We measured the intermolecular force on one collagen triple helix or a β-sheet layer translated perpendicular to the filament axis (Figure 2; see Methods). The net force, F_{tot} (in the *y*-direction), consists of the interaction force, F_{int}, directly between proteins and the water-mediated (hydration) force, F_{hyd} (Figure 4). The profile of F_{hyd} shows an

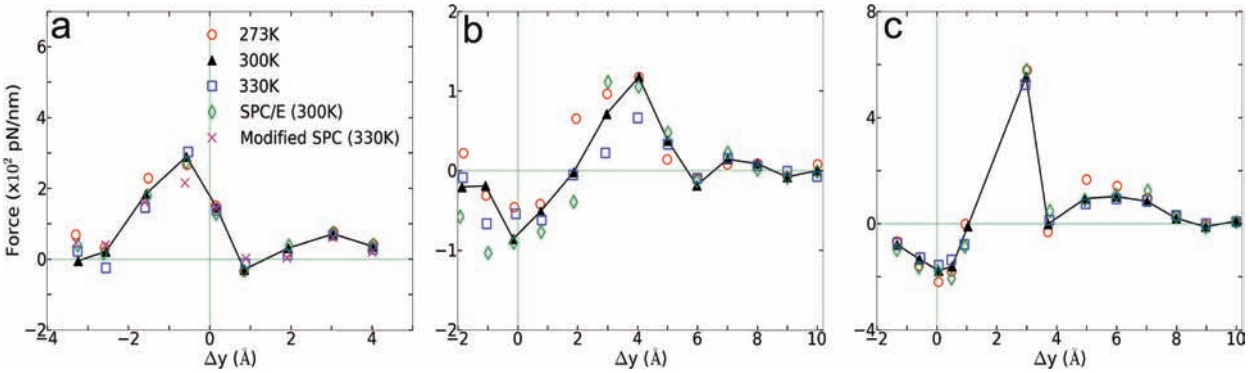

Figure 5. Comparison of hydration forces measured at different temperatures or with different water models: (a) 2D3F, (b) 2KIB, and (c) 1YJP. Temperature dependence (273, ○; 300, ▲; and 330 K, □) relates to (a) SPC and (b,c) TIP3P water models. For comparison, forces were also measured using the SPC/E water at 300 K (◇). In (a), the water oxygen and hydrogen atoms of the modified SPC (×) have 95% of the partial charges of those in the regular SPC water, to mimic the reduction in water dipole moment at high temperature.[61] The corresponding profiles of F_{tot} and F_{int} are given in Figure S13.

oscillation whose amplitude decays with Δy. The 3−4-Å oscillation period of F_{hyd} is comparable to the diameter of a water molecule, similar to the behavior between larger surfaces.[2] It should be noted that oscillation is present even between nonpolar surfaces (Figure 4b), but the location and magnitude of the hydration force peak (maximum of F_{hyd}) depend on the type of surface. In the case of collagen, which remains hydrated after assembly, the peak occurs below the crystallographic separation (Figure 4a; $\Delta y = -0.57$ Å). For β-sheet bilayers that form dry interfaces, hydration force peaks are located farther away (Figure 4b,c; $\Delta y = 3.7-4.0$ Å). The polar 1YJP has the greatest peak (553 pN/nm; force is measured per nanometer length of the filament), followed by 2D3F (289 pN/nm). Nevertheless, 1YJP forms a dry interface since the peak is formed farther away than the location of the maximum attraction of the dominant force, F_{int} (van der Waals and electrostatic; $\Delta y = 1.03$ Å).

Between the amyloid filaments, $F_{hyd} < 0$ near $\Delta y \approx 0$ Å, indicating that the surrounding water tends to prevent dissociation of β-sheets as the dry steric zipper interface is formed. This occurs for both 1YJP and 2KIB, which respectively have polar and nonpolar interfaces. Thus, ironically, the "hydrophobic" force between the β-sheets in close separation may be regarded as a manifestation of the hydration attraction. Also, due to the flat geometry of β-sheet bilayers, the attractive force per nanometer length of the 2KIB filament ($F_{hyd} = -86$ pN/nm at $\Delta y = -0.15$ Å) is greater than that for the cylindrical and hydrated collagen ($F_{hyd} = -30$ pN/nm at $\Delta y = 0.85$ Å), and it is the greatest for 1YJP ($F_{hyd} = -177$ pN/nm at $\Delta y = 0.06$ Å), whose side chains form a better steric zipper interface than 2KIB (Figure 4a−c).

The dominance of F_{int} over F_{hyd} in the β-sheet bilayers agrees with an earlier finding that the interaction energy and geometric complementary, rather than solvation free energy, are major contributors for stabilizing the amyloid steric zipper structures.[56] By contrast, in the case of collagen peptide 2D3F, since the major hydration force peak is located at the rising phase of F_{int} (Figure 4a), the interface remains hydrated after assembly. These results suggest that the three types of surfaces differ in the amplitude of the oscillating and decaying hydration force, as well as in the *phase* of oscillation relative to the equilibrium distance.

For force measurement, we used positional restraints to maintain the filaments in the original straight conformations, as in the PDB files (Figure 2). The straight conformations are due to the packing effect of filaments in the bulk,[59] which may not be the lowest in energy for small systems, as in Figure 2. Without the restraint, they develop superhelical twist. For collagen, the three peptides of 2D3F in Figure 2a mildly twist together, whereas the β-sheet bilayers become self-twisted, as reported previously.[31,60] The deformation makes it difficult to define the interfilament distance. Since our measurement reports the behavior of water for a given conformation of the filament, whether the filament is in the minimum energy conformation does not affect our main conclusions. As a result, the equilibrium position (Δy at which $F_{tot} = 0$ pN/nm) deviates from 0 Å. For crystal structures, the deviations are only 0.6 Å (2D3F) and 0.1 Å (1YJP) (Figure 4a,c), whereas the deviation is −1.3 Å for the solid-state NMR structure 2KIB (Figure 4b). The latter is consistent with the expulsion of water between the β-sheets of 2KIB in simulations without any constraint. On the other hand, the deviation in equilibrium position does not depend on the water model used in simulation (cf. Figure S13), suggesting that the deviation has a structural origin rather than being due to the limited accuracy of the force field.

For 2D3F, forces in the transverse direction (x- and z-directions) are much smaller than those in the longitudinal direction (y-direction; Figure S9a). This is also the case for 2KIB, except for $\Delta y_0 \leq 0$ Å, owing to the poor surface complementarity (Figures 2b and S9b). In 1YJP, transverse forces are much smaller than the force in the longitudinal direction, except for $\Delta y = 3-4$ Å (Figure S9c), which is due to the attraction between the Q4 side chains in the z-direction (cf. Figure S12b, white region between the two β-sheets at $\Delta y_0 = 4$ Å).

Structural Origin of the Hydration Force. Comparing between force profiles and the corresponding hydration maps reveals that the oscillation of F_{hyd} correlates strongly with the coalescence and depletion of the hydration shells. In the case of collagen, there are both dry ("*D*") and wet ("*W*") interfaces at $\Delta y_0 = 0$ Å (Figure S10). The region forming "*D*" has a single hydration shell shared between surfaces at $\Delta y_0 = 4$ Å (solid arrow in Figure 4d), which disappears by $\Delta y_0 = 1$ Å (open arrow). Similarly, in the region forming "*W*", two separate hydration shells ($\Delta y_0 = 4$ Å, double arrowhead) merge into one ($\Delta y_0 = 1$ Å, solid arrowhead), which eventually disappears ($\Delta y_0 = -3$ Å, open arrowhead). Hydration shells disrupt between these transitions at which the hydration repulsion is maximal ($\Delta y_0 = -1$ and

3 Å), but when the hydration barrier is overcome, bias toward completing the transition causes an attraction ($F_{hyd} < 0$).

The correlation between the oscillation of F_{hyd} and the coalescence/depletion of the hydration shells is also present in the β-sheet bilayers, although it is not as clearly seen due to the motion of the bulkier amino acid side chains (Figure S12). In the case of 2KIB, a low-density depletion zone is formed between the β-sheets at close separations (Figure S12a, $\Delta y_0 = 2$ Å), below which the hydration force becomes attractive (Figure 4b). This is consistent with previous reports on the dewetting transition in confined nonpolar surfaces.[8,23] However, due to the robust formation of hydration shells, dewetting does not occur at greater separations.

In contrast to the distance-dependent behavior of the hydration shells, maps for the number of hydrogen bonds or water orientation did not show any clear correlation with the hydration force profile, which we checked by going over multiple cross sections of the filament in addition to those displayed in Figures 4 and S12. Water diffusion coefficients near the protein surfaces are low in all cases. Thus, coalescence and depletion of primary hydration shells are the major determinants for the oscillatory profile of hydration force, which occurs regardless of the type of the surface. While it was necessary to apply harmonic constraints to the peptides in order to calculate forces as functions of the separation distance, since the force profile does not depend on strengths of the constraints (Methods), in their absence, major features of F_{hyd} would be preserved locally. However, the conformational motion of the molecule without a constraint will make it difficult to single out the effect of the hydration force, and it may even appear to be monotonic when averaged over the length of the filaments that have nonuniform surface separations.

Whereas the oscillation in F_{hyd} is due to the interaction between the primary hydration shells, multiple factors may affect its amplitude and phase, such as surface geometry and local hydrogen bonding events. To further illustrate the nature of the hydration force, we calculated the force profiles at 273, 300, and 330 K (Figures 5 and S13). The hydrated 2D3F has the least temperature dependence, followed by the polar 1YJP and then the nonpolar 2KIB (Figure 5). As can be seen in Figure S13b,d,f, variations in F_{int} at different temperatures are higher at shorter distances due to the stronger interaction between side chains. For β-sheets, this can be seen by the root-mean-square fluctuation of the unconstrained side-chain atoms facing the interface in the range $\Delta y_0 \leq 0$ Å. This is 0.86−1.22 Å (273−330 K) for 2KIB and 0.33−0.39 Å for 1YJP, which corroborates the size of temperature-dependent variations in F_{int}. However, at larger separations, F_{int} is independent of temperature, even though the side-chain motion increases further. Even for 2KIB, which has the greatest side-chain motion (possibly because side chains in a peptide do not flank others in the neighboring ones with the antiparallel β-sheet arrangement), F_{int} is insensitive to temperature beyond $\Delta y_0 \geq 3$ Å (Figure S13d). Thus, temperature dependence of the hydration force calculated in this range is more reliable than at shorter distances. For 2KIB, the hydration force peak appears to decrease with temperature, suggesting that its hydration shell becomes easier to disrupt with increasing temperature. While this may be due to the lack of hydrogen bonds between water and the nonpolar surface of 2KIB, since the three systems we test are not identical in surface topography, a geometry-related effect on the stability of the hydration shell cannot be ruled out.

Since the CHARMM force field we used[41] is nonpolarizable, to test whether forces are affected by temperature-dependent changes in water dipole moment,[61] for 2D3F we decreased partial charges of the water model by 5%, which yielded no major difference ($\times$ in Figures 5a and S13a). Despite the ~2-fold increase (by 95%) in diffusion coefficients of water molecules in bulk on going from 273 to 330 K, the measured hydration forces show little temperature dependence. Furthermore, the profile of F_{hyd} remained nearly the same when the SPC/E water model was used ($\diamond$ in Figures 5 and S13). Since the SPC/E water has lower diffusion coefficients than the other water models we used (Figure S1), this result further supports that hydration force does not depend on translational or rotational motion of water molecules. Although temperature dependence may become more pronounced for larger systems, possibly for 2KIB, the present results suggest that the main determinant of hydration force is the interaction between hydration shells formed by surface-induced packing of water molecules. The experimentally measured temperature dependence of the long-range attraction between collagens, DNAs, and polysaccharides[30,62] may instead be due to the conformational motion, where closer parts of the molecules interact more strongly while the average intermolecular distance is farther away, which would make the attraction appear to increase with temperature.[30,62] In contrast, experimentally measured short-range repulsion between collagens is indeed independent of temperature,[30,62] as the fluctuation effect would be less prominent. Furthermore, its magnitude is in the same range as in our simulation (Figure 4a).

CONCLUSION

The present results show that the previously postulated role of the hydration shell in generating hydration forces[13,14] is to some extent applicable to the self-assembly of filamentous proteins studied here. However, we find that the hydration shell is formed ubiquitously over all surface types in the systems tested, where differences lie in the magnitude and location of hydration repulsion and attraction, which can also be affected by the surface geometry or complementarity.[2,25] The similarity between the behaviors of the hydration water near hydrophobic and hydrophilic protein surfaces has been previously suggested,[53] although to our knowledge, its implication in hydration force has not been addressed in detail. Thus, designating a protein surface as either "hydrophobic" or "hydrophilic" may be too simplistic of a dichotomy, as surfaces in reality lie between these idealized limits.[63] There should be no fundamental difference in the way hydration forces arise among different types of protein surfaces, even with varying affinity for water.[17] Whether two surfaces eventually bind or repel will be determined by the relative magnitude and phase of hydration and interaction forces, as well as surface complementarity and flexibility. In cases where more specific interactions between amino acid side chains are involved, as in certain β-sheet filaments,[64] the ubiquitous hydration shell may serve as a "lubrication layer" that assists with the search for the specific coordination between the closely separated surfaces. While the behavior of the hydration water may be more complex for small, flexible peptides or globular proteins that have mobile subdomains,[65−67] the present results are likely applicable to a broad range of protein complexes or assemblies whose interfaces are geometrically similar to those studied here.

■ ASSOCIATED CONTENT

Supporting Information. Figure S1, comparison of hydration maps in different water models; Figure S2, definition of water orientation axes and angles; Figures S3−S5, hydration maps of the three systems tested; Figure S6, hydration maps with different strengths of constraints; Figure S7, effect of the strength of constraints on force measurement; Figure S8, correlation between the motions of protein and water; Figure S9, forces measured in transverse directions; Figure S10, dry and wet interfaces between collagens; Figure S11, potential of mean force profiles; Figure S12, hydration maps for β-sheet filaments at different distances; Figure S13, force profiles at different temperatures and with different water models; complete ref 41. This material is available free of charge via the Internet at http://pubs.acs.org.

■ AUTHOR INFORMATION

Corresponding Author
hwm@tamu.edu

■ ACKNOWLEDGMENT

We thank Alvin T. Yeh for helpful discussions. We used the Texas A&M Supercomputing Facility for simulations. This work was partly supported by grant R01GM087677 from the U.S. National Institutes of Health.

■ REFERENCES

(1) Stillinger, F. H. *Science* **1980**, *209*, 451–457.
(2) Leckband, D.; Israelachvili, J. Q. *Rev. Biophys.* **2001**, *34*, 105–267.
(3) Chaplin, M. *Nat. Rev. Mol. Cell Biol.* **2006**, *7*, 861–866.
(4) Halle, B. *Philos. Trans. R. Soc. London B* **2004**, *359*, 1207–1223.
(5) Ball, P. *Chem. Rev.* **2008**, *108*, 74–108.
(6) Lum, K.; Chandler, D.; Weeks, J. D. *J. Phys. Chem. B* **1999**, *103*, 4570–4577.
(7) Chandler, D. *Nature* **2005**, *437*, 640–647.
(8) Berne, B. J.; Weeks, J. D.; Zhou, R. *Annu. Rev. Phys. Chem.* **2009**, *60*, 85–103.
(9) Manciu, M.; Ruckenstein, E. *Langmuir* **2001**, *17*, 7582–7592.
(10) Bresme, F.; Wynveen, A. *J. Chem. Phys.* **2007**, *126*, 044501.
(11) Despa, F.; Berry, R. S. *Biophys. J.* **2007**, *92*, 373–378.
(12) Meyer, E. E.; Rosenberg, K. J.; Israelachvili, J. *Proc. Natl. Acad. Sci. U.S.A.* **2006**, *103*, 15739–15746.
(13) Israelachvili, J. *Intermolecular and surface forces*, 3rd ed.; Academic Press: London, 2010.
(14) Israelachvili, J.; Wennerström, H. *Nature* **1996**, *379*, 219–225.
(15) Eun, C.; Berkowitz, M. L. *J. Phys. Chem. B* **2009**, *113*, 13222–13228.
(16) Baron, R.; Setny, P.; McCammon, J. A. *J. Am. Chem. Soc.* **2010**, *132*, 12091–12097.
(17) Besseling, N. *Langmuir* **1997**, *13*, 2113–2122.
(18) Lu, L.; Berkowitz, M. L. *J. Chem. Phys.* **2006**, *124*, 101101.
(19) Giovambattista, N.; Lopez, C. F.; Rossky, P. J.; Debenedetti, P. G. *Proc. Natl. Acad. Sci. U.S.A.* **2008**, *105*, 2274–2279.
(20) Choudhury, N.; Pettitt, B. M. *J. Am. Chem. Soc.* **2005**, *127*, 3556–3567.
(21) Zhou, R.; Huang, X.; Margulis, C. J.; Berne, B. J. *Science* **2004**, *305*, 1605–1609.
(22) Hua, L.; Huang, X.; Zhou, R.; Berne, B. J. *J. Phys. Chem. B* **2006**, *110*, 3704–3711.
(23) Liu, P.; Huang, X.; Zhou, R.; Berne, B. J. *Nature* **2005**, *437*, 159–162.
(24) MacCallum, J. L.; Moghaddam, M. S.; Chan, H. S.; Tieleman, D. P. *Proc. Natl. Acad. Sci. U.S.A.* **2007**, *104*, 6206–6210.
(25) Cheng, Y. K.; Rossky, P. J. *Nature* **1998**, *392*, 696–699.
(26) Mittal, J.; Hummer, G. *Faraday Discuss.* **2010**, *146*, 341–352.
(27) Setny, P.; Baron, R.; McCammon, J. A. *J. Chem. Theory Comput.* **2010**, *6*, 2866–2871.
(28) Bella, J.; Brodsky, B.; Berman, H. M. *Structure* **1995**, *3*, 893–906.
(29) Kramer, R. Z.; Bella, J.; Mayville, P.; Brodsky, B.; Berman, H. M. *Nat. Struct. Biol.* **1999**, *6*, 454–457.
(30) Leikin, S.; Rau, D. C.; Parsegian, V. A. *Nat. Struct. Biol.* **1995**, *2*, 205–210.
(31) Nielsen, J. T.; Bjerring, M.; Jeppesen, M. D.; Pedersen, R. O.; Pedersen, J. M.; Hein, K. L.; Vosegaard, T.; Skrydstrup, T.; Otzen, D. E.; Nielsen, N. C. *Angew. Chem., Int. Ed.* **2009**, *48*, 2118–2121.
(32) Nelson, R.; Sawaya, M. R.; Balbirnie, M.; Madsen, A. Ø.; Riekel, C.; Grothe, R.; Eisenberg, D. *Nature* **2005**, *435*, 773–778.
(33) Sawaya, M. R.; Sambashivan, S.; Nelson, R.; Ivanova, M. I.; Sievers, S. A.; Apostol, M. I.; Thompson, M. J.; Balbirnie, M.; Wiltzius, J. J. W.; McFarlane, H. T.; Madsen, A. Ø.; Riekel, C.; Eisenberg, D. *Nature* **2007**, *447*, 453–457.
(34) Abraham, F. *J. Chem. Phys.* **1978**, *68*, 3713.
(35) Merzel, F.; Smith, J. C. *Proc. Natl. Acad. Sci. U.S.A.* **2002**, *99*, 5378–5383.
(36) Okuyama, K.; Hongo, C.; Wu, G.; Mizuno, K.; Noguchi, K.; Ebisuzaki, S.; Tanaka, Y.; Nishino, N.; Bächinger, H. P. *Biopolymers* **2009**, *91*, 361–372.
(37) Kramer, R. Z.; Bella, J.; Brodsky, B.; Berman, H. M. *J. Mol. Biol.* **2001**, *311*, 131–147.
(38) Kramer, R. Z.; Vitagliano, L.; Bella, J.; Berisio, R.; Mazzarella, L.; Brodsky, B.; Zagari, A.; Berman, H. M. *J. Mol. Biol.* **1998**, *280*, 623–638.
(39) Ravikumar, K. M.; Hwang, W. *Proteins* **2008**, *72*, 1320–1332.
(40) Spoel, D. V. D.; Lindahl, E.; Hess, B.; Groenhof, G.; Mark, A. E.; Berendsen, H. J. C. *J. Comput. Chem.* **2005**, *26*, 1701–1718.
(41) MacKerell, A. D., Jr.; et al. *J. Phys. Chem.* **1998**, *102*, 3586–3616.
(42) Anderson, D. Ph.D. thesis, University of Toronto, 2005
(43) Hess, B.; Bekker, H.; Berendsen, H.; Fraaije, J. *J. Comput. Chem.* **1997**, *18*, 1463–1472.
(44) Darden, T.; York, D.; Pedersen, L. *J. Chem. Phys.* **1993**, *98*, 10089–10092.
(45) Bussi, G.; Donadio, D.; Parrinello, M. *J. Chem. Phys.* **2007**, *126*, 014101.
(46) Berendsen, H. J. C.; Postma, J. P. M.; van Gunsteren, W. M.; DiNola, A.; Haak, J. R. *J. Chem. Phys.* **1984**, *81*, 3684–3690.
(47) Doi, M.; Edwards, S. F. *The theory of polymer dynamics*; Oxford University Press: Oxford, 1988.
(48) De Loof, H.; Nilsson, L.; Rigler, R. *J. Am. Chem. Soc.* **1992**, *114*, 4028–4035.
(49) Ravikumar, K. M.; Humphery, J. D.; Hwang, W. *J. Mech. Mater. Struct.* **2007**, *2*, 999–1010.
(50) Mark, P.; Nilsson, L. *J. Phys. Chem. A* **2001**, *105*, 9954–9960.
(51) Brooks, C. L.; Karplus, M. *J. Mol. Biol.* **1989**, *208*, 159–181.
(52) Bizzarri, A.; Cannistraro, S. *J. Phys. Chem. B* **2002**, *106*, 6617–6633.
(53) Kovacs, H.; Mark, A. E.; van Gunsteren, W. F. *Proteins* **1997**, *27*, 395–404.
(54) Russo, D.; Hura, G.; Head-Gordon, T. *Biophys. J.* **2004**, *86*, 1852–1862.
(55) Russo, D.; Ollivier, J.; Teixeira, J. *Phys. Chem. Chem. Phys.* **2008**, *10*, 4968–4974.
(56) Park, J.; Kahng, B.; Hwang, W. *PLoS Comput. Biol.* **2009**, *5*, e1000492.
(57) Makarov, V.; Pettitt, B. M.; Feig, M. *Acc. Chem. Res.* **2002**, *35*, 376–384.
(58) Schröder, C.; Rudas, T.; Boresch, S.; Steinhauser, O. *J. Chem. Phys.* **2006**, *124*, 234907.
(59) Nyrkova, I. A.; Semenov, A. N.; Aggeli, A.; Boden, N. *Eur. Phys. J. B* **2000**, *17*, 481–497.

(60) Esposito, L.; Pedone, C.; Vitagliano, L. *Proc. Natl. Acad. Sci. U.S.A.* **2006**, *103*, 11533–11538.
(61) Gubskaya, A.; Kusalik, P. *J. Chem. Phys.* **2002**, *117*, 5290–5302.
(62) Leikin, S.; Rau, D. C.; Parsegian, V. A. *Proc. Natl. Acad. Sci. U.S.A.* **1994**, *91*, 276–280.
(63) Kyte, J.; Doolittle, R. F. *J. Mol. Biol.* **1982**, *157*, 105–132.
(64) Marshall, K. E.; Morris, K. L.; Charlton, D.; O'Reilly, N.; Lewis, L.; Walden, H.; Serpell, L. C. *Biochemistry* **2011**, *50*, 2061–2071.
(65) Fenimore, P. W.; Frauenfelder, H.; McMahon, B. H.; Parak, F. G. *Proc. Natl. Acad. Sci. U.S.A.* **2002**, *99*, 16047–16051.
(66) Simone, A. D.; Dodson, G. G.; Verma, C. S.; Zagari, A.; Fraternali, F. *Proc. Natl. Acad. Sci. U.S.A.* **2005**, *102*, 7535–7540.
(67) Malardier-Jugroot, C.; Johnson, M.; Head-Gordon, T. *Phys. Chem. Chem. Phys.* **2008**, *10*, 4903–4908.